



Optics Letters

Frequency-domain Hong–Ou–Mandel interference with linear optics

POOLAD IMANY,^{1,2,*} OGAGA D. ODELE,^{1,2}  MOHAMMED S. ALSHAYKH,^{1,2} HSUAN-HAO LU,^{1,2} 
DANIEL E. LEAIRD,^{1,2} AND ANDREW M. WEINER^{1,2}

¹School of Electrical and Computer Engineering, Purdue University, West Lafayette, Indiana 47907, USA

²Purdue Quantum Center, Purdue University, West Lafayette, Indiana 47907, USA

*Corresponding author: pimany@purdue.edu

Received 29 March 2018; revised 9 May 2018; accepted 9 May 2018; posted 11 May 2018 (Doc. ID 327034); published 5 June 2018

The Hong–Ou–Mandel (HOM) interference is one of the most fundamental quantum-mechanical effects that reveal a nonclassical behavior of single photons. Two identical photons that are incident on the input ports of an unbiased beam splitter always exit the beam splitter together from the same output port, an effect referred to as photon bunching. In this Letter, we utilize a single electro-optic phase modulator as a probabilistic frequency beam splitter, which we exploit to observe HOM interference between two photons that are in different spectral modes, yet are identical in other characteristics. Our approach enables linear optical quantum information processing protocols using the frequency degree of freedom in photons such as quantum computing techniques with linear optics. © 2018 Optical Society of America

OCIS codes: (270.0270) Quantum optics; (270.5585) Quantum information and processing; (190.4410) Nonlinear optics, parametric processes.

<https://doi.org/10.1364/OL.43.002760>

The Hong–Ou–Mandel (HOM) experiment can be used as a measure of indistinguishability between two bosonic states, which leads to a nonclassical interference effect between them [1,2]. When two identical photons simultaneously arrive at the input ports of a 50/50 beam splitter—simultaneous to within the inverse of the single-photon bandwidth—four outcomes are possible: **Outcome I**, both photons get transmitted; **Outcome II**, both photons get reflected; **Outcome III**, the photon incident on input 1 of the beam splitter is transmitted while the photon in input 2 is reflected; and **Outcome IV**, the photon in input 1 gets reflected while the photon in input 2 gets transmitted. For an unbiased beam splitter, the probability of observing both photons at two different outputs of the beam splitter (**Outcomes I and II**) disappears due to destructive interference between the probability amplitudes of the photons both getting transmitted or reflected. This leads to photon bunching, meaning that the two photons always exit the beam splitter from the same port. The original work by

Hong *et al.* [1] examined this phenomenon using incident photons emanating from different spatial modes, while other properties of the photons such as polarization, and temporal and spectral modes, were identical; therefore, the concept of photon bunching in their example occurred in the spatial domain. A demonstration of the HOM interference has not been limited to photons, and has been shown with other bosonic particles such as atoms [3], phonons in trapped ions [4], and plasmons [5]. The analog of the HOM effect in fermions leads to anti-bunching as opposed to bunching in bosons, and it has been demonstrated using electrons [6] and massless Dirac fermions [7].

HOM interference is at the heart of a number of applications in quantum information processing. These applications span works such as the demonstration of fundamental optical quantum gates [8,9] necessary for quantum computation protocols [10], quantum communications [11,12], optimal quantum cloning [13], and quantum repeaters [14–16].

In this Letter, we demonstrate the photon bunching effect in a different degree of freedom, the frequency domain, where two photons in different spectral modes enter an unbiased frequency beam splitter and, at the output, they both wind up in one of the two possible output frequency modes, first proposed in Ref. [17] using strong pump beams and nonlinear interactions. Unlike prior demonstrations of frequency-domain HOM that relied on nonlinear processes to play the role of a frequency beam splitter [18,19], in our experiment, we use an electro-optic phase modulator as a frequency beam splitter, which is a linear device in the sense that its characteristics are independent of the photon flux. Consequently, our approach, compared to the use of nonlinear media, does not produce noise photons, thereby giving us a potential for better signal-to-noise ratio in our measurements.

We employ an electro-optic phase modulator as the frequency-domain analog to a spatial beam splitter. By driving the phase modulator with a radio frequency (rf) signal of the form $e^{i\delta \sin \omega_m t}$, where ω_m is the modulation frequency and δ is the modulation depth, each frequency bin projects into sidebands offset from the original center frequency by integer multiples of ω_m [20,21], making multiple comb lines out of a single frequency bin. Recently, electro-optic phase modulators

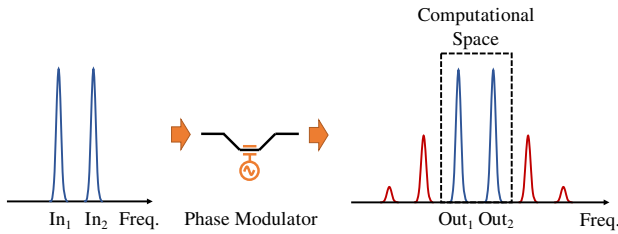


Fig. 1. Illustration of a phase modulator as a frequency beam splitter. In_1 and In_2 are the two input spectral modes to the beam splitter, and Out_1 and Out_2 are the two output modes. The red frequency bins at the output illustrate the undesired phase modulation sidebands that cause this scheme to be probabilistic.

have grown increasingly popular for frequency shifting and manipulation of single photons [22–27]. After phase modulation, the complex amplitude of the n th comb line with respect to the original frequency bin can be expressed as a Bessel function:

$$C_n = J_n(\delta), \tag{1}$$

where $J_n(\delta)$ is the Bessel function of the first kind and $J_{-n}(\delta) = (-1)^n J_n(\delta)$. The scattering matrix representing the coupling coefficients between the two input and output modes can now be written in the form

$$S = \alpha \begin{pmatrix} \frac{1}{\sqrt{2}} & \frac{1}{\sqrt{2}} \\ \frac{1}{\sqrt{2}} & -\frac{1}{\sqrt{2}} \end{pmatrix}. \tag{2}$$

Here we assume that the modulation index is chosen so that the values of $|J_n(\delta)|$ are equal for $n = -1, 0, 1$ and α accounts for transfer to other frequency modes outside our computational space. We use two frequency bins that are spaced from each other by the phase modulation frequency—these two spectral modes represent the inputs to our frequency beam splitter, as illustrated in Fig. 1. We are using the zero phase modulation sideband as the transmission and the ± 1 sidebands as the reflection ports of our frequency beam splitter. Looking at the same output spectral modes as the input modes shown as the computational space in Fig. 1, based on Eq. (1), we obtain that if the two input photons get transmitted or reflected on our beam splitter, the relative phase between these two processes is π , very much like a spatial beam splitter. This proves that a phase modulator with these specified parameters can operate as a beam splitter in the frequency domain. The red frequency bins are the phase modulation sidebands that fall outside our computational space, making this process probabilistic.

The experimental setup is depicted in Fig. 2, and an illustration of the spectrum at each step is provided in Fig. 3(a). We use a continuous-wave (CW) laser with a wavelength around

775 nm to pump a type-0 periodically poled lithium niobate waveguide. Some of the pump photons undergo spontaneous parametric down conversion to generate broadband time-frequency entangled photons with a bandwidth of ~ 5 THz around 1550 nm. The biphoton spectrum is then carved with a commercial pulse shaper to select a pair of energy-correlated signal and idler frequency bins with a 10 GHz full width at half-maximum. The line shape of these frequency bins is the convolution of a rectangular band with a Gaussian resolution function (~ 10 GHz width). The center-to-center spacing between the two frequency bins is initially set to 22 GHz. The biphotons then pass through a phase modulator driven at an rf of 22 GHz. We set the rf power so that the ± 1 phase modulation sidebands have the same power as the zero sideband, making the projection probability of the photons onto these three sidebands equal; Fig. 3(b) is a trace of the resulting phase modulation spectrum tested with a CW test laser and an optical spectrum analyzer. This causes a projection of the signal photons on the idler frequency and vice versa. Another pulse shaper routes the signal and idler frequency bins to a pair of InGaAs single photon detectors (SPDs) and, by using an event timer, we can monitor the coincidences between the SPDs.

Whenever a coincidence click appears, it must have come from a coherent superposition in which the signal and idler photons both stayed in their frequency bins during the phase modulation process (zero sideband) or they both swapped their frequency bins (± 1 sidebands). These two processes have a π phase shift with respect to each other due to the joint phase of the first sidebands with respect to the zero sideband. The terms in the two-photon state that contribute to the detection of coincidences can now be written as

$$|\psi\rangle = |\text{stay, stay}\rangle_{SI} - |\text{swap, swap}\rangle_{SI}. \tag{3}$$

The state is written in this way due to frequency indistinguishability between the $|\text{stay}\rangle$ and $|\text{swap}\rangle$ photons for both the signal and idler; therefore, if the amplitude of the two processes are the same (which we make sure of by equalizing the 0 and ± 1 phase modulation sidebands), no coincidences should be registered. Now we repeat the measurement, but with the first pulse shaper reprogrammed so that the spacings of both signal and idler frequency bins from the center of the spectrum vary from 5 to 17 GHz in 1 GHz intervals. At all times, we send the signal frequency bin and $+1$ sideband of the idler frequency bin to one detector and the idler frequency bin along with the -1 sideband from the signal frequency bin to the other detector. As the frequency spacing differs from the modulation frequency (22 GHz), the sidebands are no longer indistinguishable; hence, the coincidences start to rise. This dip in the HOM interference is observed in Fig. 3(c) in blue, with a visibility of $84\% \pm 2\%$ after accidentals subtraction, which is above the classical limit of 50% [1]. The frequency offset shown in Fig. 3(c) corresponds to the distance of the signal (idler)

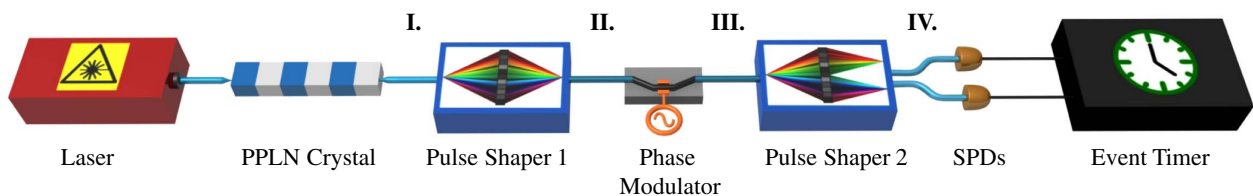


Fig. 2. Experimental setup. The Roman numerals are in reference to Fig. 3(a).

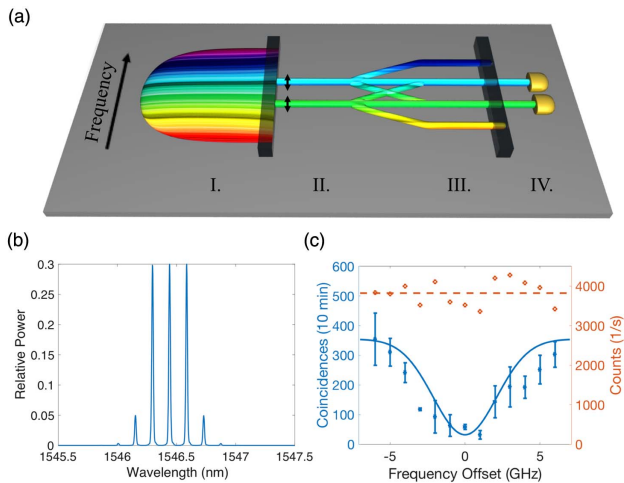


Fig. 3. (a) Illustration of the spectrum at each stage of the experiment. (b) Phase modulation spectrum of a single frequency mode. (c) HOM interference pattern in the frequency domain. The coincidences are shown in blue, and the count rates on one of the SPDs are shown in orange. The blue error bars are the measured coincidences after accidental subtraction. The subtracted accidentals were ~ 700 in a 10 min span. Each coincidence data point was measured three times to obtain the standard deviation indicated by the error bars. The blue curve is the theoretical HOM trace taking into account the 10 GHz wide signal and idler spectra of approximately Gaussian shape and the experimental visibility. The orange dashed line shows the average count rate.

frequency bin from the center of the spectrum minus half of the phase modulation frequency. The count rates on one of the SPDs is also shown in Fig. 3(c) in orange, revealing the absence of single-photon interference in our measurement. The coincidence-to-accidental ratio was about 1:2, which is poor due to the insertion loss of the components (pulse shaper, $2 \times 5 = 10$ dB; phase modulator, 2.5 dB; InGaAs SPDs, 7 dB).

We note that the imperfection in the measured visibility is due to the low coincidence-to-accidental ratio in our experimental setup, which can be improved by utilizing a lower pump power, albeit with a longer acquisition time. Unlike the nonlinear approaches proposed in [18] and [19] which use a pump to trigger frequency conversion, our frequency beam splitter does not contain a noise source, and its performance does not suffer from multiphoton components. Therefore, our HOM interference visibility does not have a theoretical imperfect limit. We also note that the frequency beam splitter used in our setup is a probabilistic splitter, in the sense that there is a probability that photons get shifted to undesired sidebands [yellow and dark blue frequency bins in stage III of Fig. 3(a)]. This indicates that after phase modulation, there is a possibility that the photons end up outside our computational basis. As can be seen in Fig. 3(b), the transmission and reflectivity of our frequency beam splitter is 0.3 for the used phase modulator setting; thus, for a single photon, 0.6 of power goes into the desired two frequency bins. Therefore, for two photons, we have a $(0.6)^2 = 0.36$ probability of both photons staying within computational space. In principle, this can be addressed by employing a more sophisticated frequency beam splitter

design which retains photons within the computational space with almost 100% success probability. As proposed in [22] and demonstrated in [23,27], instead of our single-phase modulator probabilistic frequency beam splitter, a phase modulator–pulse shaper–phase modulator sequence can be used to achieve a nearly deterministic frequency beam splitter. However, from a practical perspective, using a single-phase modulator has the advantage of lower insertion loss (by ~ 7.5 dB), compared to the reported implementation of the deterministic splitter using discrete components. If the insertion loss is taken into account, the coincidence counts achieved with our single-phase modulator frequency beam splitter should be roughly an order of magnitude higher than would be achieved with the deterministic beam splitter. On the other hand, photonic integration offers prospects for significantly reduced loss [23,25]; if these improvements in implementation can be realized, the deterministic frequency splitter approach offers better generality to support scaling to more advanced operations.

Furthermore, the resolution of our data points is limited due to the 1 GHz addressability of the pulse shaper. An alternative is to sweep the phase modulation frequency instead of the spacing between the signal and idler frequency bins. The drawback of this method is that the phase modulation depth (δ) varies with the phase modulation frequency in a very broad span (12 GHz). To ensure a constant modulation depth for each frequency value, the phase modulation spectrum will have to be adjusted by tweaking the rf power.

In summary, we used a probabilistic frequency beam splitter to demonstrate the HOM interference between single photons of different colors, using linear optical components. This experiment could contribute to the frequency processing of biphoton frequency combs [25,26], enabling optical quantum frequency gates and linear optical quantum computing protocols [28] in the frequency domain [22].

Funding. National Science Foundation (NSF) (ECCS-1407620).

Acknowledgment. The authors acknowledge Allison L. Rice for designing the graphics.

REFERENCES

1. C.-K. Hong, Z.-Y. Ou, and L. Mandel, *Phys. Rev. Lett.* **59**, 2044 (1987).
2. J.-W. Pan, Z.-B. Chen, C.-Y. Lu, H. Weinfurter, A. Zeilinger, and M. Żukowski, *Rev. Mod. Phys.* **84**, 777 (2012).
3. R. Lopes, A. Imanaliev, A. Aspect, M. Cheneau, D. Boiron, and C. I. Westbrook, *Nature* **520**, 66 (2015).
4. K. Toyoda, R. Hiji, A. Noguchi, and S. Urabe, *Nature* **527**, 74 (2015).
5. J. S. Fakonas, H. Lee, Y. A. Kelaita, and H. A. Atwater, *Nat. Photonics* **8**, 317 (2014).
6. T. Jonckheere, J. Rech, C. Wahl, and T. Martin, *Phys. Rev. B* **86**, 125425 (2012).
7. M. Khan and M. N. Leuenberger, *Phys. Rev. B* **90**, 075439 (2014).
8. J. L. O'Brien, G. J. Pryde, A. G. White, T. C. Ralph, and D. Branning, *Nature* **426**, 264 (2003).
9. T. C. Ralph, N. K. Langford, T. Bell, and A. White, *Phys. Rev. A* **65**, 062324 (2002).
10. A. Steane, *Rep. Prog. Phys.* **61**, 117 (1998).
11. H.-K. Lo, M. Curty, and B. Qi, *Phys. Rev. Lett.* **108**, 130503 (2012).
12. N. Gisin, S. Pironio, and N. Sangouard, *Phys. Rev. Lett.* **105**, 070501 (2010).

13. E. Nagali, L. Sansoni, F. Sciarrino, F. De Martini, L. Marrucci, B. Piccirillo, E. Karimi, and E. Santamato, *Nat. Photonics* **3**, 720 (2009).
14. N. Sangouard, C. Simon, H. De Riedmatten, and N. Gisin, *Rev. Mod. Phys.* **83**, 33 (2011).
15. J. Hofmann, M. Krug, N. Ortegel, L. Gérard, M. Weber, W. Rosenfeld, and H. Weinfurter, *Science* **337**, 72 (2012).
16. Z.-B. Chen, B. Zhao, Y.-A. Chen, J. Schmiedmayer, and J.-W. Pan, *Phys. Rev. A* **76**, 022329 (2007).
17. M. Raymer, S. Van Enk, C. McKinstrie, and H. McGuinness, *Opt. Commun.* **283**, 747 (2010).
18. T. Kobayashi, R. Ikuta, S. Yasui, S. Miki, T. Yamashita, H. Terai, T. Yamamoto, M. Koashi, and N. Imoto, *Nat. Photonics* **10**, 441 (2016).
19. C. Joshi, A. Farsi, and A. Gaeta, *Conference on Lasers and Electro-Optics (CLEO): QELS_Fundamental Science* (Optical Society of America, 2017), p. FF2E-3.
20. S. E. Harris, *Phys. Rev. A* **78**, 021807 (2008).
21. J. Capmany and C. R. Fernández-Pousa, *J. Opt. Soc. Am. B* **27**, A119 (2010).
22. J. M. Lukens and P. Lougovski, *Optica* **4**, 8 (2017).
23. H.-H. Lu, J. M. Lukens, N. A. Peters, O. D. Odele, D. E. Leaird, A. M. Weiner, and P. Lougovski, *Phys. Rev. Lett.* **120**, 030502 (2018).
24. L. J. Wright, M. Karpiński, C. Söller, and B. J. Smith, *Phys. Rev. Lett.* **118**, 023601 (2017).
25. P. Imany, J. A. Jaramillo-Villegas, O. D. Odele, K. Han, D. E. Leaird, J. M. Lukens, P. Lougovski, M. Qi, and A. M. Weiner, *Opt. Express* **26**, 1825 (2018).
26. M. Kues, C. Reimer, P. Roztocky, L. R. Cortés, S. Sciara, B. Wetzels, Y. Zhang, A. Cino, S. T. Chu, B. E. Little, D. J. Moss, L. Caspani, J. Azana, and R. Morandotti, *Nature* **546**, 622 (2017).
27. H.-H. Lu, J. M. Lukens, N. A. Peters, B. P. Williams, A. M. Weiner, and P. Lougovski, "Controllable two-photon interference with versatile quantum frequency processor," arXiv:1803.10712 (2018).
28. E. Knill, R. Laflamme, and G. J. Milburn, *Nature* **409**, 46 (2001).